BIOMOLECULES & THERAPEUTICS

Original Article
Biomol Ther 29(5), 527-535 (2021)

Conformational Dynamics of Sclerostin-LRP6 Complex Analyzed by HDX-MS

Yejing Jeong[1], Jinuk Kim[2], Hee-Jung Choi[2,*] and Ka Young Chung[1,*]

[1]*School of Pharmacy, Sungkyunkwan University, Suwon 16419,*
[2]*Department of Biological Sciences, Seoul National University, Seoul 08826, Republic of Korea*

Abstract

Sclerostin (SOST), a regulator of bone formation in osteocytes, inhibits the canonical Wnt signaling by interacting with low-density lipoprotein receptor-related protein 5/6 (LRP5/6) to prevent Wnt binding. Loss-of-function mutations of the *SOST* gene caused massive bone outgrowth and SOST-null mouse exhibited a high bone density phenotype. Therefore, SOST has been suggested as a promising therapeutic target for osteoporosis. A few previous studies with X-ray crystallography identified the binding interfaces between LRP6 and SOST, but there are limitations in these studies as they used truncated SOST protein or SOST peptide. Here, we analyzed the conformational dynamics of SOST-LRP6 E1E2 complex using hydrogen/deuterium exchange mass spectrometry (HDX-MS). We examined the effect of the C-terminal tail of SOST on LRP6 conformation upon complex formation. HDX-MS analysis suggested a new potential binding interface for the C-terminal region of SOST that was missing from the previous crystal structure of the SOST-LRP6 E1E2 complex.

Key Words: Low-density lipoprotein receptor-related protein 6, Sclerostin, Wnt signaling, HDX-MS

INTRODUCTION

Low-density lipoprotein (LDL) receptor-related protein 5/6 (LRP5/6) functions as a coreceptor in the canonical Wnt signaling pathway. LRP5/6 interacts with the Wnt-bound Frizzled receptor (Fzd) to induce formation of higher-order complexes called signalosomes (DeBruine *et al*., 2017). LRP6 consists of a single-pass transmembrane domain (TM), a large extracellular domain (ECD), and a cytoplasmic C-terminal domain (CTD) (Fig. 1A). The ECD contains four repeating units (E1, E2, E3, and E4), each consisting of a YWTD β-propeller domain (P1-P4) and an extracellular growth factor-like domain (EGF) (Fig. 1A, 1B) (Cheng *et al*., 2011). The LRP6 ECD serves as binding sites for Wnt ligands (i.e., Wnt3a and Wnt9b), and biochemical studies have suggested that Wnt3a and Wnt9b simultaneously interact with LRP6 by contacting LRP6 units E3E4 and E1E2, respectively (Bourhis *et al*., 2010).

In addition to Wnt ligands, Wnt signaling inhibitors such as Sclerostin (SOST) and Dickkopf-1 (DKK1) bind to the LRP6 ECD to interfere with Wnt ligand binding and inhibit Wnt signaling (Semenov *et al*., 2005; Lintern *et al*., 2009; Ahn *et al*., 2011). SOST is a secreted glycoprotein, and its loss-of-function mutation was first identified in sclerosteosis (Balemans *et al*., 2001; Brunkow *et al*., 2001). SOST is predominantly expressed in osteocytes and inhibits bone formation and growth by inhibiting Wnt signaling through LRP6 binding (Winkler *et al*., 2003; Semenov *et al*., 2005). SOST deficiency causes high bone mass and density (Brunkow *et al*., 2001; Li *et al*., 2008), indicating SOST as a promising therapeutic target for osteoporosis (Semenov and He, 2006).

The structural mechanism of SOST-LRP6 interactions is of great interest due to the clinical implications. However, the structure of the SOST-LRP6 complex was not revealed until recently (Kim *et al*., 2020). Structural studies of SOST using nuclear magnetic resonance (NMR) spectroscopy have shown that SOST forms a monomeric cystine-knot structure with three loops flanked by highly flexible N- and C-terminal regions (Fig. 1C, 1D) (Veverka *et al*., 2009; Nolan *et al*., 2013). Loop 2 of SOST has been suggested as the LRP6 binding site according to NMR spectroscopy and the crystal structure of the LRP6 E1-SOST loop 2 peptide complex (Bourhis *et al*., 2011). Moreover, recent crystal structure of the SOST-LRP6 E1E2

Open Access **https://doi.org/10.4062/biomolther.2020.234**

Received Dec 29, 2020 **Revised** Mar 19, 2021 **Accepted** Mar 22, 2021
Published Online Apr 9, 2021

***Corresponding Authors**
E-mail: choihj@snu.ac.kr (Choi HJ), kychung2@skku.edu (Chung KY)
Tel: +82-2-880-6605 (Choi HJ), +82-31-290-7787 (Chung KY)
Fax: +82-2-872-1993 (Choi HJ), +82-31-292-8800 (Chung KY)

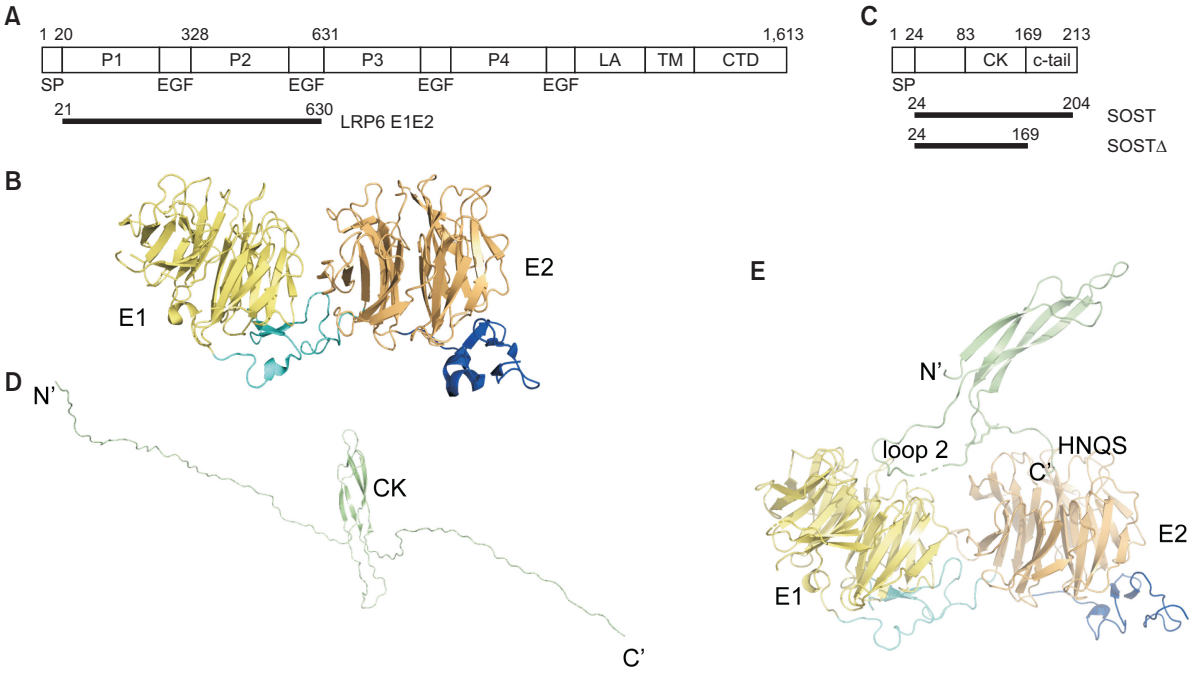

Fig. 1. Structures of LRP6 and SOST. (A) Domain scheme of LRP6. SP: signal peptide; TM: transmembrane domain; CTD: C-terminal domain. The extracellular domain contains 4 repeating units (E1-E4) that are composed of YWTD β-propeller domains (P1-P4) and an extracellular growth factor-like domain (EGF). The black bar presents the protein construct used in the current study. (B) Crystal structure of LRP6 E1E2 (PDB 3S94). (C) Domain scheme of SOST. SP: signal peptide; CK: cysteine-knot. The black bars present the protein constructs used in the current study. (D) NMR structure of SOST (PDB 2K8P). (E) Crystal structure of the SOST-LRP6 E1E2 complex (PDB: 6L6R). The N-terminal flexible 54 residues of SOST were not resolved in this structure, and the C-terminal 37 residues of SOST were truncated. Color codes for Fig. 1B, 1D, and 1E: SOST (light green), P1 within LRP6 E1 (pale yellow), P2 within LRP6 E2 (pale orange), EGF within LRP6 E1 (cyan), and EGF within LRP6 E2 (blue).

complex has shown another binding interface between LRP6 E2 and the C-terminus of SOST (Fig. 1E) (Kim *et al*., 2020). This additional binding interface explains the higher binding affinity of full-length SOST for LRP6 E1E2 compared to that of the SOST loop 2 peptide (K_D 6.8 nM vs. 9 μM) (Bourhis *et al*., 2011; Holdsworth *et al*., 2012) and the 10-fold higher affinity of LRP6 E1E2 for SOST compared to that of LRP6 E1 alone (Bourhis *et al*., 2011).

Although the newly reported crystal structure of the SOST-LRP6 E1E2 complex and related biochemical studies have revealed an additional binding interface and the role of the SOST C-terminus in inhibiting Wnt signaling (Kim *et al*., 2020), there were some limitations. First, the crystal structure was determined using the C-terminal 36 amino acid deletion mutant SOST (i.e., SOST 24-177), which does not have full activity (Fig. 1E). Thus, involvement of the SOST C-terminus in LRP6 binding was not fully elucidated by the crystal structure. Second, due to its intrinsic flexibility, the N-terminal part of SOST has not been observed in the crystal structure (Fig. 1E).

In the current study, we analyzed the effects of LRP6 E1E2-SOST complex formation on conformational dynamics using hydrogen/deuterium exchange mass spectrometry (HDX-MS). HDX-MS probes the solvent exposure of amide hydrogens, which provide conformational features to the protein.

MATERIALS AND METHODS

Materials

Insect cells were cultured with protein-free ESF 921 insect cell culture media from Expression Systems (Davis, CA, USA). Ni-NTA agarose was purchased from QIAGEN (Germantown, MD, USA). HiTrapQ column and Superdex 200 column were purchased from Cytiva (Marlborough, MA, USA). D_2O was obtained from Cambridge isotope laboratory (Tewksbury, MA, USA), TCEP from Gold Biotechnology (St. Louis, MO, USA), and guanidine hydrochloride from JUNSEI (Chuo City, Tokyo, Japan). All other chemical reagents for protein purification such as NaCl and imidazole were purchased from Sigma-Aldrich (St. Louis, MO, USA).

Protein expression and purification

Human LRP6 E1E2 (21-630) with a C-terminal 10× His tag and human SOST (24-204) with a cleavable N-terminal His_6-MBP tag were co-expressed in High Five™ insect cells (BTI-TN-5B1-4). The SOST-LRP6 E1E2 complex was purified as previously described (Kim *et al*., 2020). Briefly, secreted LRP6 E1E2 and SOST were co-purified using an Ni-NTA affinity column with an elution buffer of 50 mM Tris, pH 8.0, 300 mM NaCl, and 300 mM imidazole. After cleavage of the His_6-MBP tag by HRV3C protease, the SOST-LRP6 E1E2 complex was purified using a HiTrapQ column (Cytiva) and a size exclusion chromatography (SEC) Superdex 200 column (Cytiva). The LRP6 E1E2 – SOSTΔ (24-169) complex was purified using a

similar method.

Hydrogen/deuterium exchange (HDX) sample preparation

Protein samples were prepared at 40 μM concentrations, and HDX was initiated by mixing 8 μL of each protein sample with 22 μL or 24 μL of D_2O buffer (20 mM Tris, pD 7.4, and 200 mM NaCl) and incubating for 10, 100, 1,000, or 10,000 s on ice. The deuterated samples were quenched by adding 30 μL of ice-cold quench buffer (0.1 M NaH_2PO_4, pH 2.01, 20 mM TCEP, 1 M guanidine-HCl, and 10% glycerol), snap-frozen on dry ice, and stored at −80°C. For non-deuterated samples, 8 μL of protein samples were mixed with 24 μL of H_2O buffer (20 mM Tris, pH 7.4, and 200 mM NaCl), quenched, and frozen as described above.

HDX-MS

The quenched samples were analyzed using the HDX-UPLC-ESI-MS system (Waters, Milford, MA, USA). These samples were digested by passing through an immobilized pepsin column (2.1×30 mm) (Life Technologies, Carlsbad, CA, USA) at a flow rate of 100 μL min^{-1} with 0.05% formic acid in H_2O at 12°C. The digested fragments were collected on a C18 VanGuard trap column (1.7 μm×30 mm) (Waters) and desalted with 0.15% formic acid in H_2O. The fragments were separated by ultra-high-pressure liquid chromatography using an ACQUITY UPLC C18 column (1.7 μm, 1.0 mm×100 mm) (Waters) at a flow rate of 40 μL min^{-1} with an acetonitrile gradient starting with 8% and increasing to 85% over 8.5 min. To minimize the back-exchange of deuterium to hydrogen, buffers were adjusted to pH 2.5. Following pepsin digestion performed at 12°C, the system was maintained at 0.5°C during analysis. Mass spectra were analyzed with a Xevo G2 quadrupole-time of flight (Q-TOF) equipped with a standard electrospray ionization (ESI) source in MS^E with positive ion mode.

Peptic peptides were identified from non-deuterated samples with ProteinLynx Global Server (PLGS) 3.0 (Waters). Searches were performed with variable methionine oxidation modification. The amount of deuterium of peptic peptides was determined by measuring the centroid of the isotopic distribution using DynamX 3.0 (Waters). All data were derived from three independent experiments.

Statistical analysis

All the HDX-MS data were derived from 3 independent experiments except the following data. 10 and 1,000 s of LRP6 E1E2 alone, and 10 s of SOST-LRP6 E1E2 complex could not be obtained due to insufficient samples. The data were presented as mean ± SD.

RESULTS

HDX-MS profile changes upon SOST and LRP6 E1E2 co-incubation

To understand the role of the SOST C-terminus in LRP6 binding, we used LRP6 E1E2 (Fig. 1A) and two SOST constructs (Fig. 1C), a wild type-like 9-amino acid-deletion mutant SOST (24-204) and a C-terminal-truncated SOST (24-169) (Fig. 1C). Previously, it was shown that the C-terminal 10-amino acid-deletion mutant of SOST (24-204) was fully functional with wild-type-like activity and wild-type-like affinity for LRP6 E1E2 (Kim *et al*., 2020). Since it was difficult to overexpress and purify full-length SOST in large quantities, SOST (24-204) was used instead of full-length SOST in the HDX-MS experiment to analyze the conformational dynamics of LRP6 E1E2 upon SOST binding. Hereafter, SOST (24-204) is referred to as SOST, and SOST (24-169) with the entire C-terminal tail removed is referred to as SOSTΔ. We then investigated the HDX-MS profiles of LRP6 E1E2 alone, SOST alone, SOSTΔ alone, SOST-LRP6 E1E2 complex, and SOSTΔ-LRP6 E1E2 complex.

HDX-MS probes the exchange between amide hydrogens in a protein and deuterium in deuterated buffer. Thus, the exchange occurs faster in regions exposed to the buffer. In addition, if the amide hydrogen is protected by hydrogen bonds in helices or β-sheets, the exchange occurs slower than it does in disordered regions. Therefore, HDX-MS profiles can suggest the conformational dynamics of SOST and LRP6 E1E2 before and after complex formation. Fig. 2 shows the selected peptides used for HDX-MS analysis.

The recently published crystal structure of the SOST-LRP6 E1E2 complex suggests two binding interfaces of SOST: loop 2 and the HNQS motif located at the C-terminal extension of the core cystine-knot (Fig. 1E, 3A, red sticks) (Kim *et al*., 2020). As expected, upon complex formation, the HDX-MS profile of SOST loop 2 decreased due to weaker exposure to the buffer by binding to LRP6 E1 compared to SOST alone (Fig. 3B, peptide 116-124). Unfortunately, we could not obtain masses of peptic peptides covering the HNQS region (Fig. 2A) and thus could not analyze the HDX-MS profile of the second binding site (Fig. 3B). This could be caused by glycosylation of N175 in the HNQS motif (Kim *et al*., 2020). Instead, we obtained HDX-MS profiles of a peptic peptide next to the HNQS region (Fig. 3B, peptide 179-185), and the peptide 179-185 showed lower HDX in the complex compared to that of SOST alone (Fig. 3B). Although this region was truncated in the crystal structure of the SOST-LRP6 E1E2 complex (Fig. 1E), and the direct interaction of this region with LRP6 E1E2 was not shown, computational modeling of the SOST C-tail in complex with LRP6 E1E2 suggested that L179 and F182 may be involved in van der Waals interactions with LRP6 E2 (Kim *et al*., 2020). Thus, the current lower HDX level of region 179-185 in the complex compared to that of SOST alone supports the previous modeling data.

Previous computational modeling also suggested that a cluster of basic residues in the far C-terminal tail of SOST (residues 188-204 RPQKGRKPRPRARSAKA) interacts with LRP6 E1E2 (Kim *et al*., 2020). However, we did not detect HDX differences between SOST alone and SOST-LRP6 E1E2 complex within the far C-terminal tail of SOST in the current HDX-MS analysis (data not shown). The far C-terminal tail showed high HDX level in both states (data not shown), suggesting that this region remains disordered upon complex formation, as observed in the NMR structure of SOST alone (Fig. 1D). The discrepancy between current HDX-MS data and the previous report by Kim *et al*. (2020) could be explained by two reasons. First, the interaction may be heterogeneous and does not show clear HDX differences. Second, the interaction has been suggested to be a charge-charge interaction between acidic residues of LRP6 and positively charged residues of SOST. If this is the case, the binding may not affect buffer exposure of the amide hydrogens in this region and would not affect the HDX-MS profiles. This will be discussed

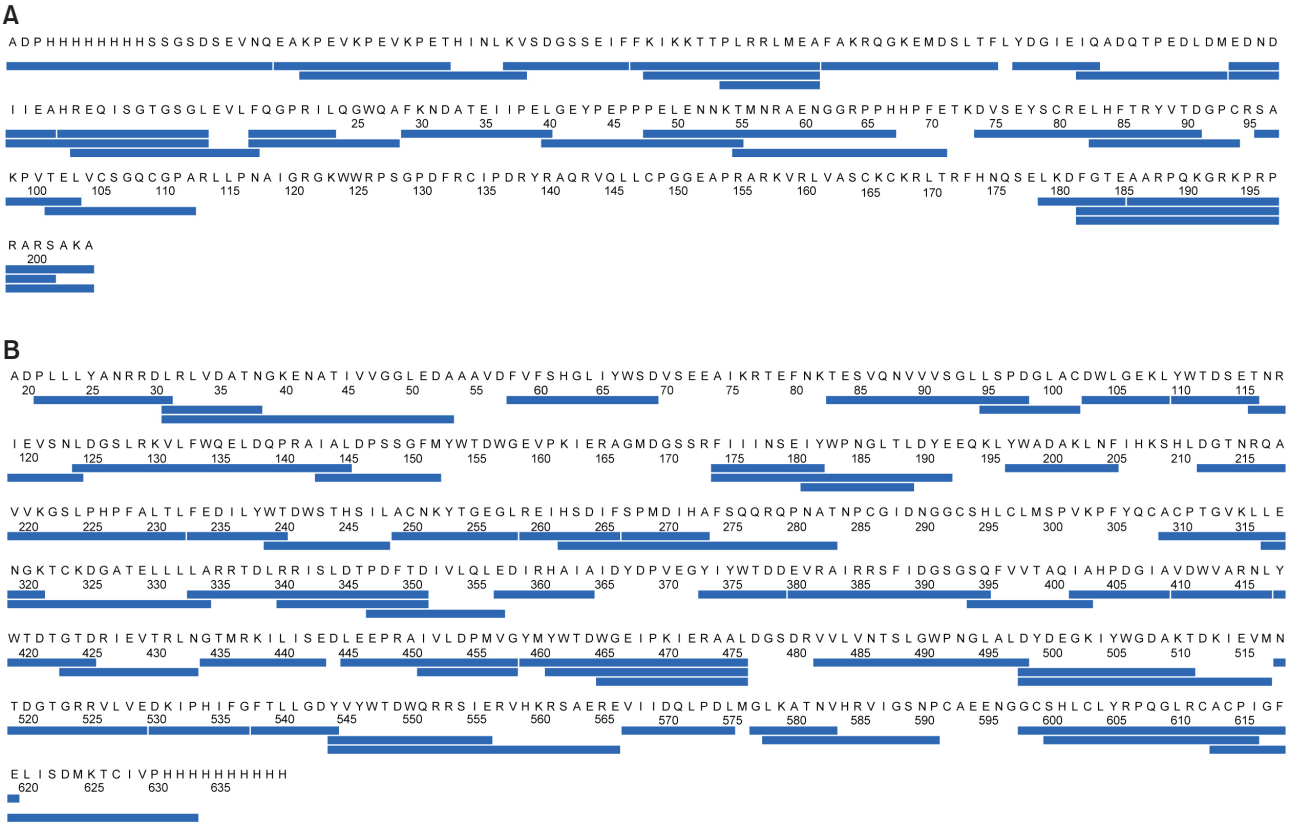

Fig. 2. Peptic peptides used for HDX-MS analysis. (A) Peptic peptides from SOST (24-204). (B) Peptic peptides from LRP6 E1E2.

below in greater detail.

Another region that showed an altered HDX-MS profile was peptide 74-91 (Fig. 3B), which is not a binding interface (Fig. 1E). Interestingly, this region showed higher HDX in the complex than in SOST alone, suggesting that this region is more flexible in the complex.

We expected that the HDX level would decrease in the binding interfaces of LRP6 E1E2 upon co-incubation with SOST. The HDX-MS analysis revealed that HDX-MS profiles of LRP6 E1E2 were affected not only within the binding interfaces, but also in regions remote from the binding interfaces (Fig. 3B, Supplementary Fig. 1). LRP6 E1E2 are in a β-propeller conformation, in which the amide hydrogens form hydrogen bonds with neighboring oxygens. The lower HDX within LRP6 E1E2 implies that SOST binding not only directly hinders solvent exposure at the binding interfaces, but also allosterically stabilizes the conformational dynamics of the β-propeller conformation in both E1 and E2.

HDX-MS profile changes upon SOSTΔ and LRP6 E1E2 co-incubation

To test the role of the C-terminal tail of SOST in complex formation, we analyzed the HDX-MS profiles upon co-incubation of SOSTΔ and LRP6 E1E2 (Fig. 4). SOSTΔ showed HDX-MS profile changes similar to SOST upon co-incubation with LRP6 E1E2; the HDX level increased in the peptide 74-91 and decreased in the peptide 116-124 (Fig. 4). The peptide 179-185 was not observed in SOSTΔ because this region was truncated (Fig. 1C).

The altered HDX levels of the peptide 116-124 from loop 2 were similar between SOST-LRP6 E1E2 and SOSTΔ-LRP6 E1E2 co-incubation samples (Fig. 3B, 4), suggesting that the binding of SOST loop 2 to the LRP6 E1 domain is similar between SOST and SOSTΔ samples. Moreover, we observed increased HDX in the peptide 74-91 in both SOST and SOSTΔ samples, which suggests that the altered conformational dynamics within residues 74-91 is because of the interaction of SOST loop 2 with LRP6 E1E2 but not by interaction of the C-terminal region of SOST.

To our surprise, SOSTΔ binding affected the HDX-MS profiles of both E1 and E2 domains of LRP6 (Fig. 4, Supplementary Fig. 2), although the C-terminal binding region of SOST that interacts with LRP6 E2 (i.e., the HNQS motif and following C-terminal tail) was truncated (Fig. 1C). This result suggests that SOST loop 2 binding at LRP6 E1 domain allosterically affects conformational dynamics of both E1 and E2 domains of LRP6.

Differences between LRP6 E1E2-SOST and LRP6 E1E2-SOSTΔ complexes

Although both LRP6 E1 and E2 domains are affected by SOSTΔ, the affected regions were slightly different from those of SOST binding (compare Supplementary Fig. 1, 2). The regions that showed distinct HDX-MS profile changes between SOST-LRP6 E1E2 and SOSTΔ-LRP6 E1E2 complexes are visualized in Fig. 5.

The current data revealed that only one region within LRP6 E2 domain (Supplementary Fig. 1, peptide 357-364) showed

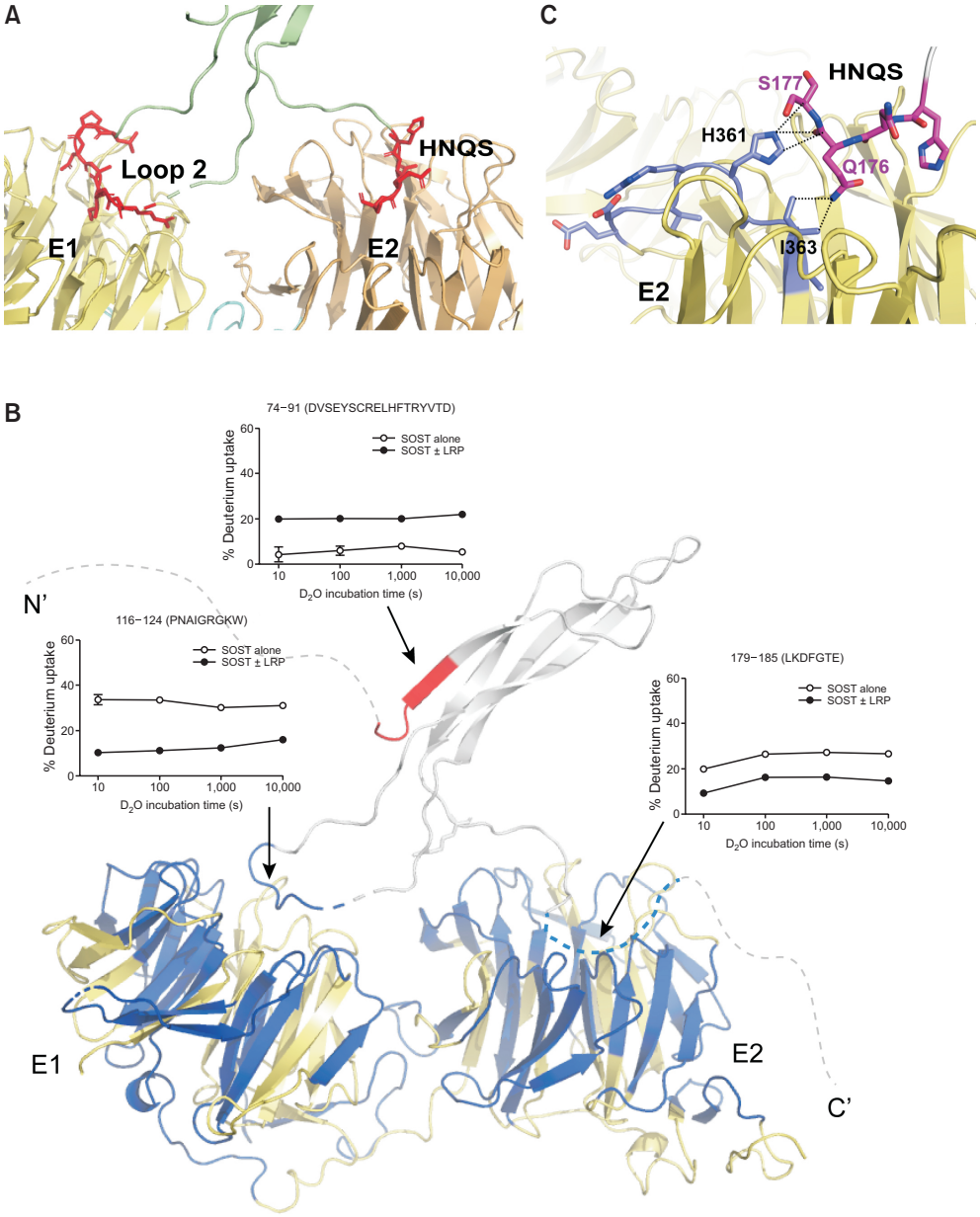

Fig. 3. HDX-MS profile changes upon SOST and LRP6 E1E2 co-incubation. (A) Two binding sites revealed by the crystal structure of the SOST-LRP6 complex (PDB: 6L6R). SOST is colored with light green, P1 within LRP6 E1 with pale yellow, and P2 within LRP6 E2 with pale orange. The SOST residues involved in binding to LRP6 E1E2 are indicated by red sticks. (B) HDX-MS profile changes upon SOST-LRP6 E1E2 co-incubation. The un-resolved regions in the crystal structure (PDB:6L6R) are shown as dotted lines. Red represents the regions that showed higher HDX in the co-incubated samples, and blue represents the regions that showed lower HDX in the co-incubated samples. Grey and yellow represent unaffected regions of SOST and LRP6 E1E2, respectively. The HDX-MS uptake plots in the figure are select SOST peptic peptides with altered HDX upon co-incubation. The HDX-MS uptake plots of LRP6 E1E2 with altered HDX upon co-incubation are summarized in Supplementary Fig. 1. (C) Interaction between the HNQS motif and LRP6 E2. The HNQS residues are indicated by magenta sticks and the side chains of LRP6 357-364 showing lower HDX in the SOST-LRP6 E1E2 complex are indicated by blue sticks. Van der Waals and polar interactions are represented as dotted lines.

distinct HDX-MS profiles change differences when comparing the SOST-LRP6 E1E2 and SOSTΔ-LRP6 E1E2 complexes (Fig. 5A, 5B, blue). Peptide 357-364 is near the binding site for the HNQS motif (Fig. 3A, 5), and especially, residues H361 and I363 of LRP6 E2 make close contacts with Q176 and S177 of SOST (Fig. 3C). This peptide showed lower HDX only in the SOST-LRP6 E1E2 complex but not in the SOSTΔ-LRP6 E1E2 complex. We also observed lower HDX with the peptide 179-185 of SOST (Fig. 3B, 5A, orange), which is next to the HNQS motif; thus, we speculate that the lower HDX of the peptide 357-364 in the SOST-LRP6 E1E2 complex was due to binding of residues 179-185 as well as the HNQS motif to this

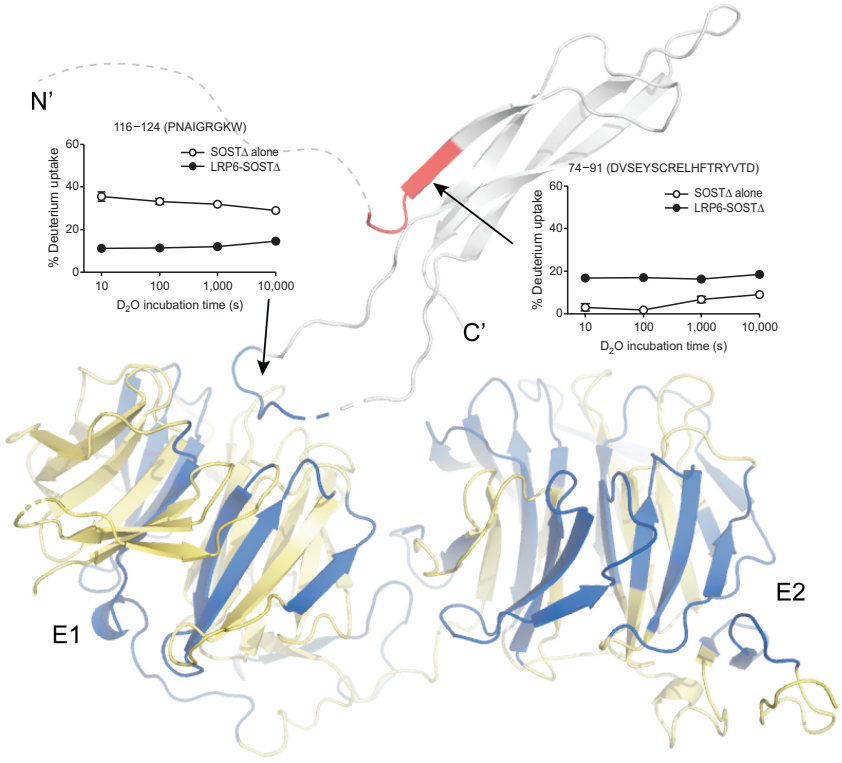

Fig. 4. HDX-MS profile changes upon C-terminal-truncated SOST (SOSTΔ) and LRP6 E1E2 co-incubation. HDX-MS profile changes upon SOSTΔ-LRP6 E1E2 co-incubation. The un-resolved regions in the crystal structure (PDB:6L6R) are shown as dotted lines. Red represents the regions that showed higher HDX in the co-incubated samples, and blue represents the regions that showed lower HDX in the co-incubated samples. Grey and yellow represent unaffected regions of SOSTΔ and LRP6 E1E2, respectively. The HDX-MS uptake plots in the figure are select SOSTΔ peptic peptides with altered HDX upon co-incubation. The HDX-MS uptake plots of LRP6 E1E2 with altered HDX upon co-incubation are summarized in Supplementary Fig. 2.

region. On the other hand, the regions within the LRP6 E2 domain that showed lower HDX levels in both SOST-LRP6 E1E2 and SOSTΔ-LRP6 E1E2 complexes (Fig. 4, blue colored region in E2 domain) would be so affected because binding of SOST loop 2 at the LRP6 E1 domain allosterically stabilizes the conformational dynamics of the LRP6 E2 domain.

Computational modeling has suggested that the far C-terminal tail interacts at the side of the β-propeller domain of LRP6 E2 (residues E529, D530, E564, E556, E566, and D570) (Kim *et al*., 2020). However, we did not detect HDX-MS profile change differences in this region between the SOST-LRP6 E1E2 and SOSTΔ-LRP6 E1E2 complexes (Fig. 5). As described above, we did not detect HDX-MS profile changes in the far C-terminal tail of SOST upon SOST-LRP6 E1E2 complex formation (Fig. 3B). The absence of difference in HDX-MS profile changes in the LRP6 E2 domain between the SOST-LRP6 E1E2 and SOSTΔ-LRP6 E1E2 complexes could be explained as follows. First, as mentioned above, a charge-charge interaction between LRP6 E2 and a basic-residue cluster in the SOST C-tail would likely not affect buffer exposure of the amide hydrogens. Second, this interaction might not be residue-specific. LRP6 is an acidic protein that contains several acidic patches on its surface. Although Kim *et al*. (2020) specified some acidic residues of LRP6 E2 for SOST C-tail binding by computational modeling, this ionic interaction may not be residue-specific. Rather, any acidic residues on the LRP6 surface could be potential binding sites for the SOST C-tail. In fact, computational modeling proposed three binding modes (two are similar) (Kim *et al*., 2020).

Interestingly, we observed that a number of regions within LRP6 E1 showed decreased HDX profiles only in the SOST-LRP6 E1E2 complex but not in the SOSTΔ-LRP6 E1E2 complex (Fig. 5, cyan-colored regions, Supplementary Fig. 1, 2; peptides 31-53, 95-102, 212-232, and 239-248). It is not clear what caused decreased HDX in these regions of LRP6 E1 upon complex formation. It is unlikely that these regions are the direct binding sites for the far C-terminal tail of SOST, because the C-terminal region of SOST did not show the measurable binding affinity to LRP6 E1, while it binds to LRP6 E1E2 with a K_D of 5.8 μM (Kim *et al*., 2020). As we observed HDX-MS changes in LRP6 E2 when SOSTΔ binds to LRP6 E1, SOST C-tail binding at LRP6 E2 may allosterically affect the conformational dynamics of LRP6 E1. Further investigation is needed to understand the structural dynamics of LRP6 E1E2 upon SOST binding.

DISCUSSION

The current study analyzed the conformational changes of SOST and LRP6 E1E2 upon complex formation using HDX-MS. In our HDX-MS experiment, we identified loop 2 of SOST as a binding interface, consistent with the previous study (Kim *et al*., 2020) (Fig. 6B, 6C). We also investigated the role of the

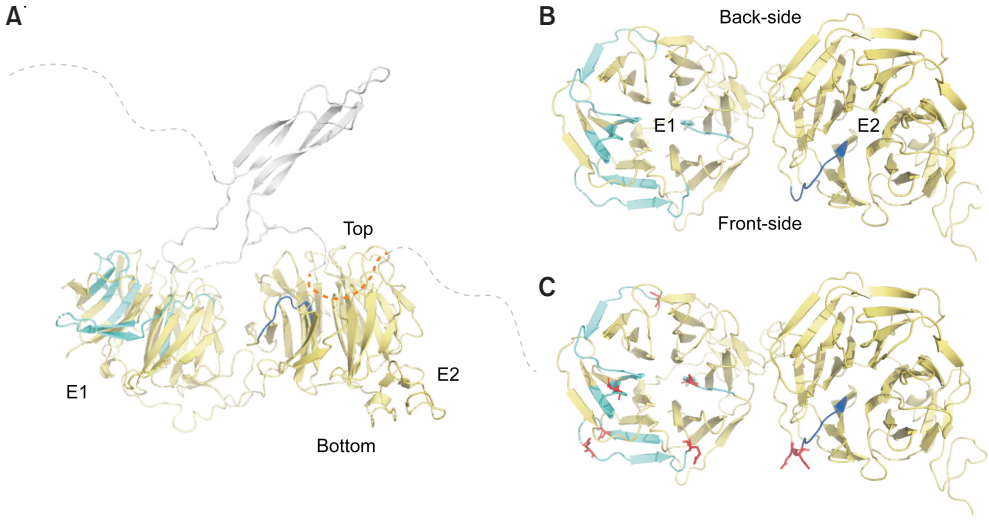

Fig. 5. HDX-MS profile change differences between SOST-LRP6 E1E2 and SOSTΔ-LRP6 E1E2 complexes. (A) Regions with distinct HDX-MS profile changes between SOST-LRP6 E1E2 and SOSTΔ-LRP6 E1E2 complexes. Grey and yellow represent unaffected regions of SOST and LRP6 E1E2, respectively. Cyan, blue, and orange represent regions that showed lower HDX upon complex formation within E1, E2, and SOST, respectively, in the SOST-LRP6 E1E2 complex but not in the SOSTΔ-LRP6 E1E2 complex. (B) Top view of LRP6 E1E2 from Fig. 5A. (C) Negatively charged residues within the regions with distinct HDX-MS profile changes are shown as red sticks.

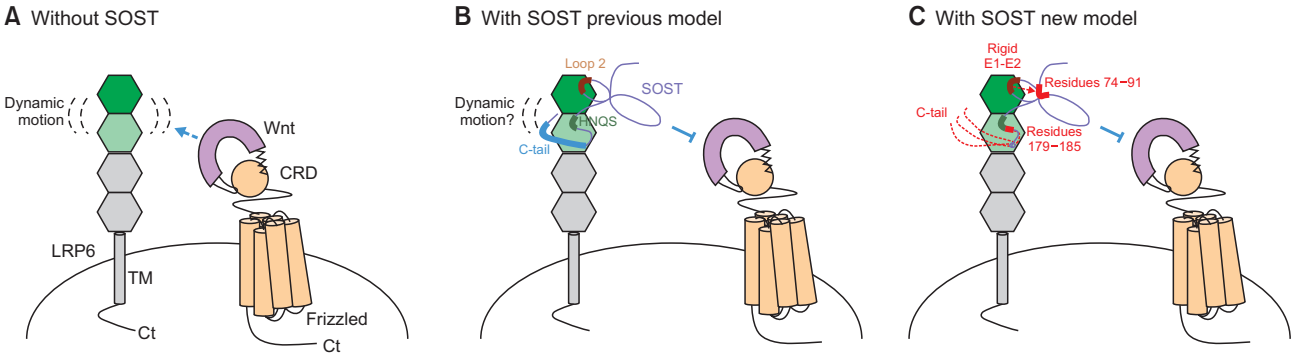

Fig. 6. Proposed mechanism of SOST-LRP6 E1E2 interaction. (A) In the absence of SOST, Wnt signaling is activated by binding of Wnt ligand to Frizzled receptor and LRP6 E1E2 domain. Without SOST binding, LRP6E1E2 is in dynamic motion. (B) Previous model of SOST-LRP6 E1E2 binding (Kim *et al*., 2020). Loop 2, HNQS, and C-tail of SOST are the major binding interfaces to LRP6 E1E2, and the binding of SOST to LRP6 prevents Wnt ligand binding to LRP6 resulting in inhibition of Wnt signaling. (C) Newly suggested model of SOST-LRP6 E1E2 binding. The newly suggested binding interfaces and allosteric conformational changes are highlighted with red.

C-terminal part of SOST by analyzing HDX-MS data upon co-incubation of LRP6 E1E2 and SOSTΔ. These data suggested dynamic allosteric conformational changes of LRP6 and SOST upon complex formation and a potential novel binding interface between LRP6 E2 and the near C-terminal part of SOST (i.e., regions next to the HNQS motif) (Fig. 6C).

Previously, the C-terminal part of SOST was studied separately as two distinct regions. One is the HNQS motif (residues 174-177), and the other is a basic cluster in the far C-terminal region (RPQKGRKPRPRARSAKA, residues 188-204) (Fig. 6B) (Kim *et al*., 2020). The HNQS motif was identified by the crystal structure of the SOST-LRP6 E1E2 complex and functional analysis, while the far C-terminal region was suggested by computational modeling and mutational studies. Although we could not analyze regions containing the HNQS motif, we did obtain HDX-MS data for a region next to the HNQS motif (residues 179-185). The failure to obtain peptides containing the HNQS motif is likely due to the glycosylation of N175. The region next to the HNQS motif (residues 179-185) showed reduced HDX upon complex formation. The binding site within LRP6E1E2 for the residues 179-185 would be speculated by analyzing HDX-MS data of LRP6E1E2. Comparison of the HDX-MS data of SOST-LRP6 E1E2 and SOSTΔ-LRP6 E1E2 complexes showed that the HDX level within residues 357-364 of LRP6 E2 was decreased only in the SOST-LRP6 E1E2 complex but not SOSTΔ-LRP6 E1E2 complex. Interestingly, H361 of LRP6 E2 forms a polar interaction with the carbonyl of Q176 of SOST and H361 and I363 of LRP6 E2 form van der Waals interactions with Q176 and S177 of SOST (Fig. 3C). These results imply that residues 179-185 of SOST and residues 357-364 of LRP6 E2 form a binding interface that extends continuously from the binding interface mediated by

the HNQS motif of SOST (Fig. 6C).

Unexpectedly, we did not observe HDX level differences within the far C-terminal region between non-complexed and complexed samples. Moreover, we did not detect HDX differences at the potential binding site of the far C-terminal region within LRP6 E2 as suggested by computer simulation, between SOST-LRP6 E1E2 and SOSTΔ-LRP6 E1E2 complexes. This may be because the interaction mediated by the far C-terminal region is heterogeneous, making it difficult to detect by HDX-MS (Fig. 6C).

The most interesting finding of the current study is allosteric conformational changes upon complex formation. Residues 74-91 of SOST, which span a region far from the binding interfaces, showed increased HDX in both SOST-LRP6 E1E2 and SOSTΔ-LRP6 E1E2 complexes. This result suggests that this region became more dynamic upon complex formation, and the conformational change is due to allosteric effects propagated from binding of SOST loop 2 to LRP6 E1 (Fig. 6C). The potential allosteric route from loop 2 to residues 74-91 would be through a flexible part before the LRP6 E1 binding residues 116-124 (residues 106-115). Although we did not detect HDX profile changes in this region probably because the amide hydrogens were not affected, we speculate that binding of the loop 2 affects the conformation of this region which affects the conformational dynamics of neighboring residues 74-91. Carefully designed experiments are needed to test this hypothesis.

LRP6 E1E2 also showed profound allosteric conformational changes upon complex formation (Fig. 6A, 6C). HDX level was affected not only in the binding interfaces, but also in remote regions. Comparison of the HDX-MS data of SOST-LRP6 E1E2 and SOSTΔ-LRP6 E1E2 complexes revealed that interaction of SOST loop 2 with LRP6 E1 allosterically affects not only LRP6 E1, but also LRP6 E2. Similarly, SOST C-terminal region binding to LRP6 E2 would affect the conformational dynamics of LRP6 E1. These allosteric conformational changes resulted in less dynamic (rigid) motion of LRP6 E1E2 (Fig. 6C). A few previous reports suggested that tandem domains allosterically affect each other, and these allosteric structural effects affect the physiological function of the protein (Giladi *et al*., 2015). Further study is needed to investigate the physiological effects of allosteric conformational changes on LRP6 signaling.

Previous structural and functional studies have suggested that SOST loop 2 and the C-terminal region are the major binding site for LRP6 E1 and E2, respectively (Fig. 6B). The previous work also has revealed that SOSTΔ showed ~5-fold lower affinity for LRP6 E1E2 than SOST and reduced activity for inhibition of Wnt1 signaling (Kim *et al*., 2020), and these results were explained by the fact that the C-terminal part of SOST interacts at LRP6 E2. The current study proposes a novel binding site (i.e., interaction between the region next to the HNQS motif of SOST and LRP6 E2) and more precise binding mode of the C-tail of SOST (Fig. 6C). Moreover. We further suggest that there are more profound allosteric conformational changes resulting in rigidified motion of LRP6 E1E2 upon SOST binding (Fig. 6C). These newly suggested mode explain more about the increases the binding affinity of SOST to LRP6 E1E2. The increased binding affinity enhances the inhibitory effect of SOST for the Wnt-LRP6 complex formation by increased competitive binding.

Therefore, our work adds to the knowledge of precise binding mechanisms between SOST and LRP6. The data provided by this current study should prove useful in targeting of SOST for treating bone diseases such as osteoporosis (Lewiecki, 2011; MacNabb *et al*., 2016).

CONFLICT OF INTEREST

There is no conflict of interest.

ACKNOWLEDGMENTS

This research is supported by the National Research Foundation of Korea, funded by the Korean government (grant numbers NRF-2018R1A2B6001554 and NRF-2019R1A5A2027340 to K.Y.C. and NRF-2020R1A2C2003783 to H.-J.C.).

REFERENCES

Ahn, V. E., Chu, M. L., Choi, H. J., Tran, D., Abo, A. and Weis, W. I. (2011) Structural basis of Wnt signaling inhibition by Dickkopf binding to LRP5/6. *Dev. Cell* **21**, 862-873.

Balemans, W., Ebeling, M., Patel, N., Van Hul, E., Olson, P., Dioszegi, M., Lacza, C., Wuyts, W., Van Den Ende, J., Willems, P., Paes-Alves, A. F., Hill, S., Bueno, M., Ramos, F. J., Tacconi, P., Dikkers, F. G., Stratakis, C., Lindpaintner, K., Vickery, B., Foernzler, D. and Van Hul, W. (2001) Increased bone density in sclerosteosis is due to the deficiency of a novel secreted protein (SOST). *Hum. Mol. Genet.* **10**, 537-543.

Bourhis, E., Tam, C., Franke, Y., Bazan, J. F., Ernst, J., Hwang, J., Costa, M., Cochran, A. G. and Hannoush, R. N. (2010) Reconstitution of a frizzled8.Wnt3a.LRP6 signaling complex reveals multiple Wnt and Dkk1 binding sites on LRP6. *J. Biol. Chem.* **285**, 9172-9179.

Bourhis, E., Wang, W., Tam, C., Hwang, J., Zhang, Y., Spittler, D., Huang, O. W., Gong, Y., Estevez, A., Zilberleyb, I., Rouge, L., Chiu, C., Wu, Y., Costa, M., Hannoush, R. N., Franke, Y. and Cochran, A. G. (2011) Wnt antagonists bind through a short peptide to the first beta-propeller domain of LRP5/6. *Structure* **19**, 1433-1442.

Brunkow, M. E., Gardner, J. C., Van Ness, J., Paeper, B. W., Kovacevich, B. R., Proll, S., Skonier, J. E., Zhao, L., Sabo, P. J., Fu, Y., Alisch, R. S., Gillett, L., Colbert, T., Tacconi, P., Galas, D., Hamersma, H., Beighton, P. and Mulligan, J. (2001) Bone dysplasia sclerosteosis results from loss of the SOST gene product, a novel cystine knot-containing protein. *Am. J. Hum. Genet.* **68**, 577-589.

Cheng, Z., Biechele, T., Wei, Z., Morrone, S., Moon, R. T., Wang, L. and Xu, W. (2011) Crystal structures of the extracellular domain of LRP6 and its complex with DKK1. *Nat. Struct. Mol. Biol.* **18**, 1204-1210.

DeBruine, Z. J., Xu, H. E. and Melcher, K. (2017) Assembly and architecture of the Wnt/beta-catenin signalosome at the membrane. *Br. J. Pharmacol.* **174**, 4564-4574.

Giladi, M., Lee, S. Y., Hiller, R., Chung, K. Y. and Khananshvili, D. (2015) Structure-dynamic determinants governing a mode of regulatory response and propagation of allosteric signal in splice variants of Na+/Ca2+ exchange (NCX) proteins. *Biochem. J.* **465**, 489-501.

Holdsworth, G., Slocombe, P., Doyle, C., Sweeney, B., Veverka, V., Le Riche, K., Franklin, R. J., Compson, J., Brookings, D., Turner, J., Kennedy, J., Garlish, R., Shi, J., Newnham, L., McMillan, D., Muzylak, M., Carr, M. D., Henry, A. J., Ceska, T. and Robinson, M. K. (2012) Characterization of the interaction of sclerostin with the low density lipoprotein receptor-related protein (LRP) family of Wnt co-receptors. *J. Biol. Chem.* **287**, 26464-26477.

Kim, J., Han, W., Park, T., Kim, E. J., Bang, I., Lee, H. S., Jeong, Y.,

Roh, K., Kim, J., Kim, J. S., Kang, C., Seok, C., Han, J. K., Choi, H. J. (2020) Sclerostin inhibits Wnt signaling through tandem interaction with two LRP6 ectodomains. *Nat. Commun.* **11**, 5357.

Lewiecki, E. M. (2011) Sclerostin monoclonal antibody therapy with AMG 785: a potential treatment for osteoporosis. *Expert Opin. Biol. Ther.* **11**, 117-127.

Li, X., Ominsky, M. S., Niu, Q. T., Sun, N., Daugherty, B., D'Agostin, D., Kurahara, C., Gao, Y., Cao, J., Gong, J., Asuncion, F., Barrero, M., Warmington, K., Dwyer, D., Stolina, M., Morony, S., Sarosi, I., Kostenuik, P. J., Lacey, D. L., Simonet, W. S., Ke, H. Z. and Paszty, C. (2008) Targeted deletion of the sclerostin gene in mice results in increased bone formation and bone strength. *J. Bone Miner. Res.* **23**, 860-869.

Lintern, K. B., Guidato, S., Rowe, A., Saldanha, J. W. and Itasaki, N. (2009) Characterization of wise protein and its molecular mechanism to interact with both Wnt and BMP signals. *J. Biol. Chem.* **284**, 23159-23168.

MacNabb, C., Patton, D. and Hayes, J. S. (2016) Sclerostin antibody therapy for the treatment of osteoporosis: clinical prospects and challenges. *J. Osteoporos.* **2016**, 6217286.

Nolan, K., Kattamuri, C., Luedeke, D. M., Deng, X., Jagpal, A., Zhang, F., Linhardt, R. J., Kenny, A. P., Zorn, A. M. and Thompson, T. B. (2013) Structure of protein related to Dan and Cerberus: insights into the mechanism of bone morphogenetic protein antagonism. *Structure* **21**, 1417-1429.

Semenov, M., Tamai, K. and He, X. (2005) SOST is a ligand for LRP5/LRP6 and a Wnt signaling inhibitor. *J. Biol. Chem.* **280**, 26770-26775.

Semenov, M. V. and He, X. (2006) LRP5 mutations linked to high bone mass diseases cause reduced LRP5 binding and inhibition by SOST. *J. Biol. Chem.* **281**, 38276-38284.

Veverka, V., Henry, A. J., Slocombe, P. M., Ventom, A., Mulloy, B., Muskett, F. W., Muzylak, M., Greenslade, K., Moore, A., Zhang, L., Gong, J., Qian, X., Paszty, C., Taylor, R. J., Robinson, M. K. and Carr, M. D. (2009) Characterization of the structural features and interactions of sclerostin: molecular insight into a key regulator of Wnt-mediated bone formation. *J. Biol. Chem.* **284**, 10890-10900.

Winkler, D. G., Sutherland, M. K., Geoghegan, J. C., Yu, C., Hayes, T., Skonier, J. E., Shpektor, D., Jonas, M., Kovacevich, B. R., Staehling-Hampton, K., Appleby, M., Brunkow, M. E. and Latham, J. A. (2003) Osteocyte control of bone formation via sclerostin, a novel BMP antagonist. *EMBO J.* **22**, 6267-6276.